



Cite this: *Soft Matter*, 2025, 21, 5947

Received 25th February 2025,
Accepted 24th June 2025

DOI: 10.1039/d5sm00201j

rsc.li/soft-matter-journal

Defect dynamics in dry active nematics by residue calculus for holomorphic functions of nematic director field

Hiroki Miyazako,^{ID}*† Hiroyuki Miyoshi† and Takaaki Nara

This paper proposes a theory for modeling the dynamics of topological defects in dry active nematics. We introduce a holomorphic function for integral curves of the director field and show the density of the integral curves corresponds to that of active nematic liquid crystals such as confined spindle-shaped cells. Then, we derive equations of motion for defects by considering active stress defined from the integral curves. A mathematical analysis of the equations reveals that the dynamics of the defects can be explicitly expressed with the residues of holomorphic functions derived from the director field. We verify the proposed theory using existing work on the motion of a defect pair and demonstrate estimation of parameters for active stress by cell culture experiments.

1 Introduction

Recent studies in the field of biophysics and non-equilibrium physics have revealed that living or actively moving nematic liquid crystals induce complex fluidic and mechanical phenomena known as active nematics.^{1–3} The complex behavior of active nematics is governed by topological defects, at which the alignment of nematic liquid crystals cannot be defined. Active stress induced by components of an active nematic system creates a force acting on topological defects, resulting in self-propelled motion of the defects. Many studies have investigated the dynamics of defect motion for various active nematic systems such as compounds of kinesins and microtubules,^{4–8} spindle-shaped cell populations^{9–20} and morphogenesis of *Hydra*.^{21,22}

To theoretically explain the complex behavior of active nematics, many studies applied complex analysis,^{23–38} because the alignment of nematic liquid crystals can be expressed by complex logarithmic functions under the one-constant approximation in liquid crystal theories.³⁹ Complex analysis has enabled the explicit expression of the alignment of nematic liquid crystals^{24,27,30–33} and the force and torque acting on topological defects.^{23,25,26,28,29,35–38} According to the explicit expressions based on complex analysis, equations for defect motion have been derived, which allow a detailed theoretical analysis of defect behaviors.

Theoretical studies of defect motion have considered passive and active stresses caused by the elasticity and mechanical deformation of nematic liquid crystals, respectively, and the equations of motion were then derived from the force acting on defects by the passive stress and Stokes flow caused by the active stress to model “wet” active nematics where the conservation of momentum is considered.^{23,37} In these studies, the density of the active nematic liquid crystals was assumed to be constant for simplicity in the theoretical calculations. On the other hand, the densities of the components tend to be non-uniform around topological defects in actual active nematic systems. Such non-uniformity is often observed in cell populations at a confluent state; for example, neural progenitor cells show aggregation and escape behaviors around $+1/2$ and $-1/2$ defects, around which the cell alignment angle changes by $+180^\circ$ and -180° , respectively.¹¹ In addition, some studies reported observations of extrusion of spatially confined cells around a $+1/2$ defect in MDCK cells¹⁰ and a $+1$ defect in mouse myoblast cells.¹² These studies support the non-uniformity of components of cell populations which can be viewed as “dry” active nematic systems,¹ where substrate friction is dominant and thus the conservation of momentum does not hold. To theoretically study the dynamics of topological defects in cell populations, new theoretical approaches are necessary to consider the non-uniform distribution of components in dry active nematics.

The aim of this study is to develop a theoretical framework for defect motion in dry active nematic systems that considers the orientational continuity and density of liquid crystals in a simple manner. To this end, we extend the work of Vitelli and Nelson, who introduced a complex potential to express such

Department of Information Physics and Computing, Graduate School of Information Science and Technology, The University of Tokyo, 7-3-1, Hongo, Bunkyo-ku, Tokyo, Japan. E-mail: hiroki_miyazako@ipc.i.u-tokyo.ac.jp

† These authors contributed equally to this work.



continuous lines from a holomorphic function for nematic alignment.⁴⁰ We show that such a formalism provides an explicit expression of active stress based on holomorphic functions and that the densities of the constructed continuous lines increase and decrease around $+1/2$ and $-1/2$ defects, respectively, which is qualitatively consistent with the experimental observations of cell populations in the literature.¹¹ In addition, we demonstrate that the proposed formalism enables both mathematical analyses of defect motion and the prediction of the active stress parameter from cell culture experiments.

This paper is organized as follows. In Section 2, we introduce a holomorphic function for modeling density of liquid crystals around topological defects by extending the work of Vitelli and Nelson.⁴⁰ In Section 3, we show that the active stress can be explicitly expressed by the introduced holomorphic function defined in Section 2. In Section 4, we demonstrate the validity of the proposed theory using existing work on the motion of a defect pair studied by Giomi *et al.*²³ In Section 5, we consider the confinement of liquid crystals in simply connected domains and show that the proposed theory can be extended to the confined geometries considered in existing studies.^{9,16,20} In Section 6, we show that the extended theory for confined nematic liquid crystals can be applied to the prediction of the active stress parameter from cell culture experiments.

The mathematical notation in this paper is as follows. \mathbb{Z} , \mathbb{R} and \mathbb{C} represent the sets of integers, and real and complex numbers, respectively. For a complex number $z \in \mathbb{C}$, the real and imaginary parts of z are expressed as $\text{Re}[z]$ and $\text{Im}[z]$, respectively. $\mathbb{D} := \{\zeta \in \mathbb{C} | |\zeta| < 1\}$ denotes the open unit disk in the complex ζ -plane.

2 Complex function theory for nematic director field around topological defects

First, we consider the alignment of nematic liquid crystals in the complex plane $z = x + iy$, whose director field is defined as $\mathbf{n}_d(x, y) = (\cos \phi(x, y), \sin \phi(x, y))^T$. We assume that the size of the nematic liquid crystals is neglected. Since the nematic liquid crystals are non-polar molecules, we assume that the alignment angle ϕ is defined in the quotient space $\mathbb{R}/\pi\mathbb{Z}$; that is, ϕ is equivalent to $\phi + m\pi$ for any $m \in \mathbb{Z}$. In this paper, we consider the one-constant approximation from liquid crystal theory,³⁹ which allows us to assume that the alignment angle $\phi(x, y)$ is harmonic. Then, the alignment angle $\phi(x, y)$ can be expressed by taking the real part of a holomorphic function $f(z) = \phi(x, y) + i\psi(x, y)$, where $\psi(x, y)$ is a conjugate harmonic function of $\phi(x, y)$. Based on the report of Vitelli and Nelson,⁴⁰ we can construct continuous lines whose tangential orientation at (x, y) is parallel to the orientation of the director field $\mathbf{n}_d(x, y)$ according to the following procedures. Let us consider a following holomorphic function defined from $f(z)$:

$$h'(z) = A \exp(-if(z)) = Ae^{\psi}(\cos \phi - i \sin \phi) \quad (1)$$

where $' \equiv \frac{d}{dz}$ and A is an arbitrary real non-zero constant. Since the coefficient Ae^{ψ} is real, the vector field $\mathbf{n}_h(x, y) = (Ae^{\psi} \cos \phi, Ae^{\psi} \sin \phi)^T$ defined from (1) represents the director field scaled by the factor Ae^{ψ} . Thus, we refer to the vector field $\mathbf{n}_h(x, y)$ as the holomorphic director field in this paper. Accordingly, $h(z)$ is called the complex potential for the holomorphic director field.

By considering the contours of the imaginary part of $h(z)$, we can obtain the integral curves of the holomorphic director field $\mathbf{n}_h(x, y)$,⁴⁰ whose tangential orientation is parallel to the orientation of the director field $\mathbf{n}_d(x, y)$. That is, the integral curves are given by the following contour line:

$$\text{Im}[h(z)] = c \quad (c \in \mathbb{R}). \quad (2)$$

This fact is proven mathematically by the following procedure. For a line element ds on (2), we have

$$\frac{d}{ds} \text{Im}[h(z)] = \text{Im} \left[\frac{d}{ds} h(z) \right] = \text{Im} \left[\frac{dz}{ds} h'(z) \right] = 0. \quad (3)$$

It holds from (1) and (3) that

$$A \cdot \text{Im} \left[\frac{dz}{ds} e^{\psi} e^{-i\phi} \right] = Ae^{\psi} \text{Im} \left[\frac{dz}{ds} e^{-i\phi} \right] = 0. \quad (4)$$

Using $|dz/ds| = 1$ and (4), we have $dz/ds = e^{i\phi}$ or $dz/ds = -e^{i\phi} = e^{i(\phi+\pi)}$. Since ϕ and $\phi + \pi$ are equivalent in the quotient space $\mathbb{R}/\pi\mathbb{Z}$, the tangential derivative dz/ds is parallel to the director field $\mathbf{n}_d(x, y)$ on the contour line $\text{Im}[h(z)] = c$. This means the tangential direction at $z = x + iy$ on the contour line $\text{Im}[h(z)] = c$ is parallel to the director field $\mathbf{n}_d(x, y)$. We refer to the contours of $\text{Im}[h(z)]$ as integral curves of the holomorphic director field $\mathbf{n}_h(x, y)$ (hereinafter, referred to simply as integral curves).

In the following, we investigate the mathematical and physical meaning of the constructed integral curves for some simple examples. When the nematic liquid crystals are aligned along the real axis, $\phi(x, y)$ is equal to zero for all z , which means $f(z) = 0$ and $h'(z) = A \exp(-if(z)) = A$. Then, the complex potential $h(z)$ is equal to $Az + c$, where c is an arbitrary constant and we set $c = 0$ throughout this paper without loss of generality. Since the imaginary part of $h(z)$ is Ay , the contour lines are parallel to the real axis and uniformly distributed as shown in Fig. 1(a). Note that the density of the contour lines in Fig. 1(a) differs according to the absolute value of A because the slope of the contour lines is A . Thus, the parameter $|A|$ represents the density of the integral curves when there are no topological defects in the space.

Next, we consider the alignment around a topological defect around which the alignment angle changes by $2\pi q$, where q is a half or full non-zero integer, called the topological charge. In this case, the alignment angle around the defect is expressed as the real part of $f(z) = -iq \log z$. Then, the complex potentials $h(z)$ around a defect with topological charges of $q = +1/2$ and $-1/2$ are given as follows:

$$h(z) = \begin{cases} iAz^{1/2} & (q = +1/2), \\ iAz^{3/2} & (q = -1/2). \end{cases} \quad (5)$$

We refer to these two defects as $+1/2$ and $-1/2$ defects in this



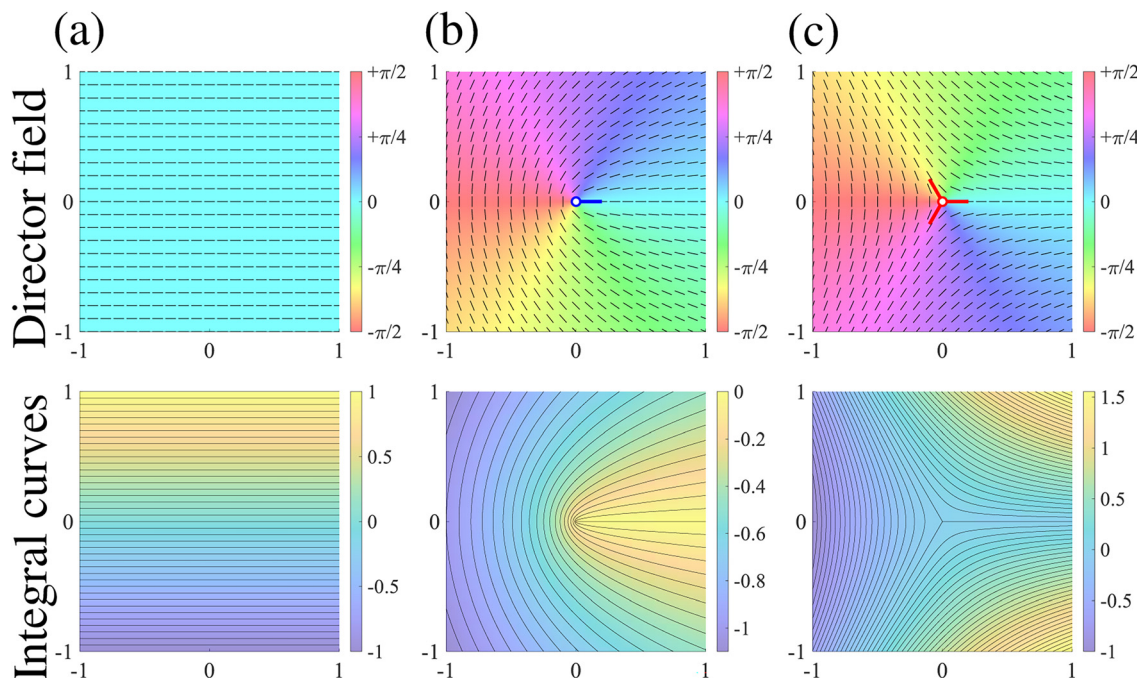


Fig. 1 Schematics of director field and integral curves. (a) No defect. (b) $+1/2$ defect. (c) $-1/2$ defect. The black lines in the director field and integral curves indicate the orientation of the director and contours of $\text{Im}[h(z)]$, respectively. The contour interval is 0.05.

paper. The contours of $\text{Im}[h(z)]$ are shown in Fig. 1(b) and (c). In contrast to Fig. 1(a), the contours around the $+1/2$ and $-1/2$ defects become denser and sparser toward the origin, respectively.

The difference in the density occurs because the density of the contours of $\text{Im}[h(z)] \equiv \Psi(x, y)$ is proportional to the magnitude of its gradient $|\nabla\Psi(x, y)| = |h'(z)|$. For $\pm 1/2$ defects, the gradient in polar coordinates $z = re^{i\theta}$ is calculated as

$$|\nabla\Psi| = |h'(re^{i\theta})| = \begin{cases} Ar^{-1/2} & (+1/2 \text{ defect}), \\ Ar^{1/2} & (-1/2 \text{ defect}). \end{cases} \quad (6)$$

Thus, when we consider the limit of $r \rightarrow 0$, $|h'(z)|$ diverges to $+\infty$ for $q = +1/2$ whereas $|h'(z)|$ converges to 0 for $q = -1/2$, which is consistent with Fig. 1(b) and (c).

Note that the non-uniform density of the integral curves around $+1/2$ defects is qualitatively consistent with experiments on active nematics in extrusion of MDCK cells¹⁰ and aggregation of neural progenitor cells around $+1/2$ defects.¹¹ Thus, the proposed formulation is a plausible approach for the theoretical investigation of dry active nematics from the viewpoint of the density of the integral curves.

3 Representations of passive and active stresses by residue calculus

In the following section, we investigate the representation of passive and active stresses in studying the dynamics of defect motion driven by forces acting on topological defects. For this, we assume that N topological defects exist in the complex z -plane. Then, the director of the nematic alignment is

expressed by

$$f(z) = -\sum_{k=1}^N iq_k \log(z - z_k) + \phi_0, \quad (7)$$

where $\phi_0 \in \mathbb{R}$ is some real constant, and z_k and q_k are the location and topological charge of the k -th defect, respectively. We also denote a small disk with a radius of ε that includes only a k -th defect as $D_k(\varepsilon)$, which is referred to as a defect core. According to Giomi *et al.*,²³ we have to consider two forces due to elastic and active stress. For the elastic stress, Denniston⁴¹ derived the passive force $(F_x^p, F_y^p)^T$ in a complex form for the topological defect located at $z = z_k$ as follows:

$$F_x^p - iF_y^p = 2\pi iq_k K \frac{\partial \hat{f}_k}{\partial z}(z_k) = \frac{iK}{2} \oint_{\partial D_k(\varepsilon)} f'(z)^2 dz, \quad (8)$$

where K is the Frank elastic constant and $\hat{f}_k(z) \equiv f(z) + iq_k \log(z - z_k)$ is a function $f(z)$ except for the logarithmic singularity at $z = z_k$. This formula is also applicable to simply and doubly connected domains with infinite anchoring conditions on the boundaries.⁴²

On the other hand, the active stress generated by self-propelled particles is expressed as

$$\sigma^a = \alpha c^2 S \begin{pmatrix} \cos 2\phi & \sin 2\phi \\ \sin 2\phi & -\cos 2\phi \end{pmatrix}, \quad (9)$$

where S is the scalar order parameter, c is the concentration of the particles and α is a constant that is positive or negative for contractile or extensile motion, respectively.^{23,43} Note that the existing studies^{23,43} assumed that the density of the self-propelled particles was constant, which implies that the spatial



change in the force was not explicitly considered. To appropriately model the non-uniformity of the force around topological defects, the density of the integral lines of the holomorphic director field \mathbf{n}_h should be considered. This consideration is reasonable because the driving force for active nematics is generated by extensile or contractile behaviors of elongated cells, which can be viewed as the integral lines of \mathbf{n}_h . To this end, we consider the force generated by self-propelled particles on the integral lines and assume that the density of self-propelled particles on a line is proportional to the density of the integral lines. Since the density of the integral lines is proportional to $|h'(z)| = e^\psi$, as discussed above, we assume that the concentration c in (9) is proportional to e^ψ . The active stress tensor for the holomorphic director field \mathbf{n}_h is then given by

$$\hat{\sigma}^a = \frac{\alpha}{2} e^{2\psi} \begin{pmatrix} \cos 2\phi & \sin 2\phi \\ \sin 2\phi & -\cos 2\phi \end{pmatrix}. \quad (10)$$

In (10), the scalar order parameter S is merged into α because S is assumed to be constant outside the defect core $D_k(\varepsilon)$ in theoretical analyses.²⁸ In addition, the parameter α is rescaled to $\alpha/2$ to simplify the following calculation.

Using the derived stress tensor $\hat{\sigma}^a$, the active force applied to defects can be explicitly expressed in the same way as the elastic force derived by Denniston.⁴¹ The force applied to $D_k(\varepsilon)$ is given by

$$\left(F_x^a, F_y^a \right)^T = \oint_{\partial D_k(\varepsilon)} \hat{\sigma}^a \hat{\mathbf{n}} ds, \quad (11)$$

where $\hat{\mathbf{n}}$ is a normal vector on the boundary $\partial D_k(\varepsilon)$. Using $\hat{\mathbf{n}} = (\cos \theta, \sin \theta)^T$ on the point $z = z_k + \varepsilon e^{i\theta} \in \partial D_k(\varepsilon)$ and applying a direct calculation, the force due to active stress is

$$\begin{aligned} F_x^a - iF_y^a &= \frac{\alpha\varepsilon}{2} \int_0^{2\pi} e^{2\psi} (\cos \theta e^{-2i\phi} + i e^{-2i\phi} \sin \theta) d\theta \\ &= -\frac{i\alpha}{2} \oint_{\partial D_k(\varepsilon)} h'(z)^2 dz, \end{aligned} \quad (12)$$

where we used $dz = i\varepsilon e^{i\theta} d\theta$. It follows from (8) and (12) that the

force acting on the defect is given by the following formula

$$F_x - iF_y = \frac{i}{2} \oint_{\partial D_k(\varepsilon)} [Kf'(z)^2 - \alpha h'(z)^2] dz. \quad (13)$$

This formula means that the forces acting on defects are determined by residues of the two holomorphic functions $f'(z)^2$ and $h'(z)^2$, which are derived from the two director fields $\mathbf{n}_d(x, y)$ and $\mathbf{n}_h(x, y)$, respectively.

4 Theoretical analyses on motion of a defect pair

Based on the derived formula for the forces, the equations of defect motion can be explicitly expressed as follows. In this treatment, we consider the defect dynamics of the dry active nematics, where the substrate friction is dominant and thus the conservation of the momentum does not hold. According to the existing study of Duclos *et al.*,⁹ the substrate friction is dominant in confined cell populations, which means the defect dynamics in confined cell populations can be modeled as dry active nematics. The defect dynamics of dry active nematics, where the effects of hydrodynamics are neglected, can be expressed using the following overdamped equation of motion:

$$\zeta_f \frac{d\bar{z}_j}{dt} = F_x - iF_y, \quad (14)$$

where ζ_f is a frictional constant.²³ To verify consistency with the work of Giomi *et al.*,²³ we consider the case of two topological defects with opposite signs on an infinite plane. The holomorphic function for the director field $\mathbf{n}_d(x, y)$ is given by

$$f(z) = -\frac{i}{2} \log(z - z_1(t)) + \frac{i}{2} \log(z - z_2(t)) - \frac{\pi}{2}, \quad (15)$$

where $z_1(t)$ and $z_2(t)$ are the positions of the defects with charges of $\pm 1/2$ at time t , and the alignment angle becomes $\pi/2$ in the far-field. By definition, we have

$$h'(z) = iA \sqrt{\frac{z - z_2(t)}{z - z_1(t)}}. \quad (16)$$

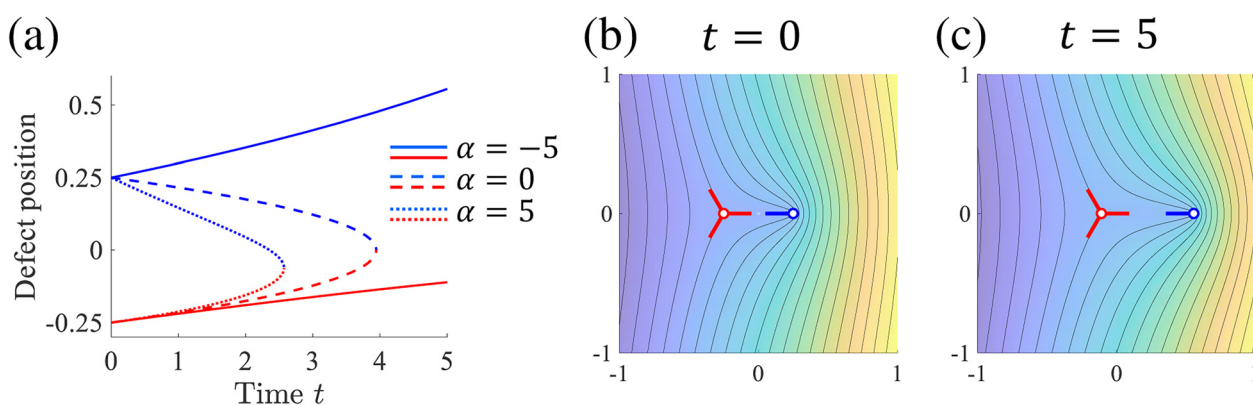


Fig. 2 Motion of a defect pair. (a) Time evolution of $z_1(t)$ and $z_2(t)$ for $K = 1$, $A = 1$ and $\zeta_f = 100$. The blue and red lines represent $z_1(t)$ and $z_2(t)$, respectively. (b) and (c) Integral curves around the defect pair for $\alpha = -5$ calculated from (17).



The integral curves around the defect pair are obtained by analytically integrating (16) with respect to z , which gives

$$h(z) = iA \left[(z_1(t) - z_2(t)) \sinh^{-1} \left(\sqrt{\frac{z - z_1(t)}{z_1(t) - z_2(t)}} \right) + z \sqrt{(1 - z_1(t)/z)(1 - z_2(t)/z)} \right]. \quad (17)$$

Calculating the residues of $f'(z)^2$ and $h'(z)^2$ at each defect, the equations of motion are derived as follows:

$$\zeta_f \frac{dz_1(t)}{dt} = -\frac{\pi K}{2(z_1(t) - z_2(t))} - \pi \alpha A^2 (z_1(t) - z_2(t)) \quad (18)$$

$$\zeta_f \frac{dz_2(t)}{dt} = +\frac{\pi K}{2(z_1(t) - z_2(t))} \quad (19)$$

The solutions of (18) and (19) simulate the temporal movement of the two defects, as shown in Fig. 2(a). Fig. 2(b) and (c) show a typical behavior of extensile motion ($\alpha < 0$). Because of the active stress term with negative α , the topological defect with $+1/2$ moves away from the other defect, which follows the distortion of the integral curves around the $+1/2$ defect.

It is difficult to analytically solve the simultaneous differential eqn (18) and (19). However, the dynamics of the pair separation $\Delta(t) := x_1(t) - x_2(t)$ can be solved in closed form under the assumption that the two defects are located on the real axis. By subtracting (19) from (18), the differential equation of the separation $\Delta(t)$ is given by

$$\begin{aligned} \frac{d\Delta(t)}{dt} &= -\frac{\pi \alpha A^2}{\zeta_f} \Delta(t) - \frac{\pi K}{\zeta_f \Delta(t)} \\ &= v_0 \frac{\Delta(t)}{\Delta(0)} - \frac{2\kappa}{\Delta(t)} \\ &= \frac{2\kappa}{\Delta(0)} \left(\lambda \frac{\Delta(t)}{\Delta(0)} - \frac{\Delta(0)}{\Delta(t)} \right), \end{aligned} \quad (20)$$

where $v_0 := -\pi \alpha A^2 \Delta(0)/\zeta_f$, $\kappa := \pi K/(2\zeta_f)$ and $\lambda := v_0 \Delta(0)/2\kappa$. Since the derived eqn (20) is in the form of a Bernoulli differential

equation when $\alpha \neq 0$, (20) is analytically solved as follows:

$$\begin{aligned} \Delta(t) &= \sqrt{\left(\Delta(0)^2 + \frac{K}{\alpha A^2} \right) \exp\left(-\frac{2\pi \alpha A^2}{\zeta_f} t \right) - \frac{K}{\alpha A^2}} \\ &= \sqrt{\left(\Delta(0)^2 - \frac{2\kappa}{v_0} \Delta(0) \right) \exp\left(\frac{2v_0}{\Delta(0)} t \right) + \frac{2\kappa}{v_0} \Delta(0)}. \end{aligned} \quad (21)$$

The solid lines in Fig. 3(a) show the typical time course of the solution (21) when the contractile active stress (*i.e.* $v_0 \propto -\alpha < 0$) is considered. The annihilation time shortens as the constant κ increases. Moreover, the annihilation of the defect pair can be predicted by setting the right-hand side of the solution (21) equal to zero. When $\alpha > -K/(A^2 \Delta(0)^2)$, the defect pair is annihilated at the following time T_a :

$$\begin{aligned} T_a &= \frac{\zeta_f}{2\pi \alpha A^2} \log \left(1 + \alpha \frac{A^2 \Delta(0)^2}{K} \right) \\ &= -\frac{\Delta(0)}{2v_0} \log \left(1 - \frac{v_0 \Delta(0)}{2\kappa} \right) \end{aligned} \quad (22)$$

In the limit of $\alpha \rightarrow 0$, the annihilation time becomes $T_a^0 = \zeta_f \Delta(0)^2 / (2\pi K) = \Delta(0)^2 / 4\kappa$, which is consistent with the annihilation of a defect pair in passive nematic systems.²³ The annihilation time normalized by T_a^0 depends only on the non-dimensional quantity $\lambda = v_0 \Delta(0)/2\kappa$ as follows:

$$\frac{T_a}{T_a^0} = -\frac{1}{\lambda} \log(1 - \lambda). \quad (23)$$

Fig. 3 shows the relationship between the parameter $-\lambda$ and the normalized annihilation time (23).

We next compare the derived differential eqn (20) with the existing work of Giomi *et al.*²³ According to Giomi *et al.*, the equation of the pair separation $\Delta(t)$ is given as follows:

$$\begin{aligned} \frac{d\Delta(t)}{dt} &= v_0 - \frac{2\kappa}{\Delta(t)}, \\ &= \frac{2\kappa}{\Delta(0)} \left(\lambda - \frac{\Delta(0)}{\Delta(t)} \right), \end{aligned} \quad (24)$$

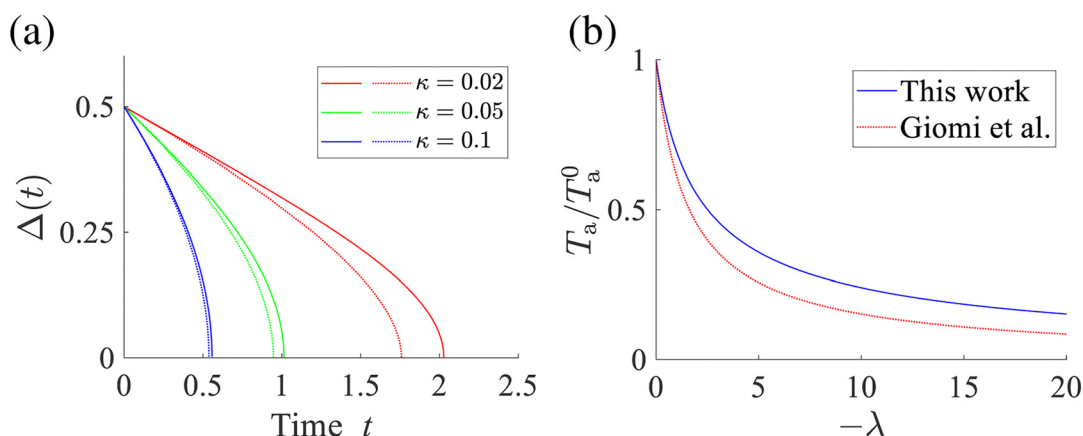


Fig. 3 Dynamics of the defect separation when contractile active stress is considered. (a) Time course of the defect separation $\Delta(t)$ for $v_0 = -0.1$ and various constants κ . The solid and dotted lines represent the solutions of the eqn (20) and (24), respectively. To solve (24), ode23s in MATLAB[®] was used. (b) Relationship between the parameter $-\lambda$ and the normalized annihilation time T_a/T_a^0 .



where $v_0 \propto -\alpha$ is the constant self-propelled velocity of the +1/2 defect, $\kappa := \pi K/(2\zeta_f)$ and $\lambda := v_0\Delta(0)/2\kappa$. The dotted lines in Fig. 3 show the solutions of (24) and indicate that the annihilation time for (24) shortens compared to that for (20) when the same parameters v_0 , κ and $\Delta(0)$ are used. The normalized annihilation time for (24) is calculated as follows:

$$\begin{aligned} \frac{T_a}{T_a^0} &= \frac{4\kappa}{\Delta(0)^2} \left(-\frac{\Delta(0)}{v_0} - \frac{2\kappa}{v_0^2} \log \left(1 - \frac{v_0}{2\kappa} \Delta(0) \right) \right) \\ &= -\frac{2}{\lambda} - \frac{2}{\lambda^2} \log(1 - \lambda). \end{aligned} \quad (25)$$

The normalized annihilation time for (24) is always less than that for (20) as shown in Fig. 3. This difference between (20) and (24) is due to the first term in the right-hand side, which is derived from the active stress. Specifically, the first term in (24) is constant, whereas that in (20) is proportional to the normalized separation $\Delta(t)/\Delta(0)$. Thus, the contribution of the active stress in the proposed model (20) becomes small when $\Delta(t)$ goes to zero, whereas the contribution of the active stress in (24) remains constant even when $\Delta(t)$ goes to zero. As the contribution of the contractile active stress enhances the annihilation of defect pairs, the normalized annihilation time for (24) will become shorter than that for (20). This difference in the first term may be critical when the two defects are far away from each other. However, the comparison between our and Giomi's results (Fig. 3) implies that the difference between the two models is not significant, with the same trend of defect pair annihilation reproduced in the proposed model, which indicates there is not a serious gap between the proposed theory and Giomi's model when the defects are located close to each other.

Note that the above difference between our and Giomi's approaches is due to the difference between dry and wet active nematics, respectively. Giomi *et al.* considered the flow dynamics induced by the active and passive stresses and then solved the dynamics of the defect pair, whereas we neglected the hydrodynamics and considered that the velocities of the defects are directly proportional to the forces acting on the defects. Thus, our approach cannot be applied to the complex behaviors of active turbulence observed in compounds of microtubules and kinesins^{4–8} because the conservation of

momentum should be considered in such active fluid. Though the proposed model can consider only dry active nematics, it has an advantage from the viewpoint of analytic calculations. Since Giomi *et al.* considered the Stokes flow induced by the external active stress around a single defect, they needed to calculate the line integrals regarding the Oseen tensor. This approach would be more difficult for more complex defect configurations, such as defects in confined geometries. In contrast, our formalism focuses on direct calculation of the forces acting on defects, which results in a simple evaluation of the residues of the holomorphic functions at each defect. This simplified approach allows us to investigate the motion of defects of confined cell populations in more complicated domains, as will be discussed in the following section.

5 Equilibrium states of topological defects in confined geometries

We investigate the equilibrium states of defect motion in confined geometries, which have been investigated for elongated cell populations.^{9,10,12,16,20} Specifically, we consider two +1/2 defects located at $\zeta = \zeta_1, \zeta_2$ in a unit disk \mathbb{D} , with its image mapped by a conformal mapping of $z = g(\zeta)$. According to our previous studies,^{20,32} the holomorphic function for the director field $\mathbf{n}_d(x, y)$ in $\Omega := g(\mathbb{D})$ is expressed by

$$f_\Omega(z) = f_{\mathbb{D}}(g^{-1}(z)) - i \log g'(g^{-1}(z)), \quad (26)$$

where $f_{\mathbb{D}}(\zeta)$ is the holomorphic function of the director field in \mathbb{D} given by

$$f_{\mathbb{D}}(\zeta) = -\frac{i}{2} \sum_{k=1}^2 [\log(\zeta - \zeta_k) + \log(1 - \bar{\zeta}_k \zeta)] - \frac{\pi}{2}. \quad (27)$$

From (1) and (27), we have

$$\begin{aligned} h'_{\mathbb{D}}(\zeta) &= \exp(-if_{\mathbb{D}}(\zeta)) \\ &= \frac{i}{\sqrt{(\zeta - \zeta_1)(\zeta - \zeta_2)(1 - \bar{\zeta}_1 \zeta)(1 - \bar{\zeta}_2 \zeta)}}. \end{aligned} \quad (28)$$

Thus, the complex potential for the holomorphic director field

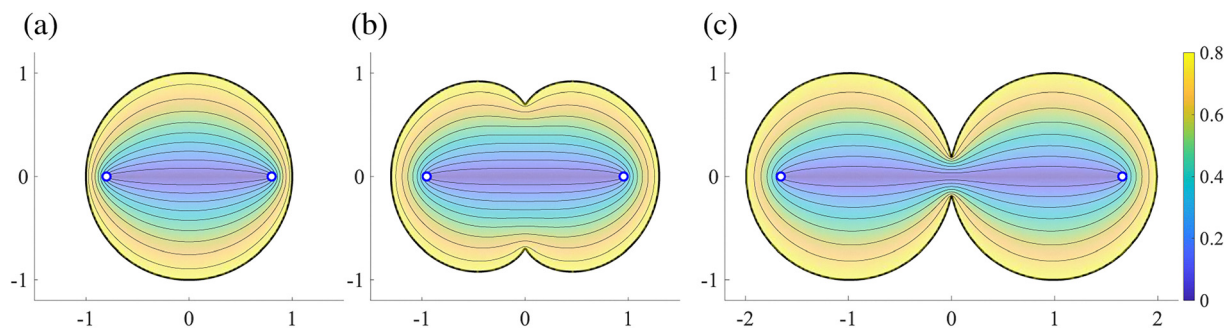


Fig. 4 Integral curves in confined geometries. (a) Unit disk \mathbb{D} . (b) Domain Ω mapped from the unit disk by the function $g(\zeta) = \zeta + 0.3\zeta^3$. (c) Domain Ω mapped from the unit disk by the function $g(\zeta) = \frac{a^4 - 1}{a^2 - a + 1} \cdot \frac{\zeta}{a^2 - \zeta^2}$, where $a = 1.1$.



in \mathbb{D} is obtained by

$$h_{\mathbb{D}}(\zeta) = \frac{2iF(\hat{\eta}|\hat{m})}{\sqrt{(1-|\zeta_1|^2)(1-|\zeta_2|^2)}}, \quad (29)$$

where $F(\eta|m) := \int_0^\eta d\theta / \sqrt{1-m^2 \sin^2 \theta}$ is an incomplete elliptic integral of the first kind and

$$\hat{\eta} = \sin^{-1} \left(\sqrt{\frac{(\zeta - \zeta_1)(1 - \zeta_2 \bar{\zeta}_2)}{(\zeta - \zeta_2)(1 - \zeta_1 \bar{\zeta}_2)}} \right), \quad (30)$$

$$\hat{m} = \frac{(1 - \zeta_2 \bar{\zeta}_1)(1 - \zeta_1 \bar{\zeta}_2)}{(1 - \zeta_1 \bar{\zeta}_1)(1 - \zeta_2 \bar{\zeta}_2)}. \quad (31)$$

Fig. 4(a) shows the integral lines of the derived potential $h_{\mathbb{D}}(\zeta)$. The line density around the $+1/2$ defects increases, which is similar to Fig. 1.

Using the derived potential $h_{\mathbb{D}}(\zeta)$, the complex potential in the mapped domain $\Omega = g(\mathbb{D})$ can be calculated as follows. It follows from the definition (1) that

$$\begin{aligned} \frac{dh_{\Omega}(z)}{dz} &= \exp(-if_{\Omega}(z)) = \exp(-if_{\mathbb{D}}(\zeta) - \log g'(\zeta)) \\ &= \frac{1}{g'(\zeta)} \exp(-if_{\mathbb{D}}(\zeta)). \end{aligned} \quad (32)$$

Then, we have

$$\begin{aligned} h_{\Omega}(z) &= \int^z \frac{dh_{\Omega}(\hat{z})}{d\hat{z}} d\hat{z} \\ &= \int^{\zeta} \frac{1}{g'(\zeta)} \exp(-if_{\mathbb{D}}(\zeta)) g'(\zeta) d\zeta \\ &= h_{\mathbb{D}}(\zeta). \end{aligned} \quad (33)$$

Eqn (33) means that the complex potential for the holomorphic director field $h(z)$ is conformally invariant, whereas the holomorphic function associated with the director field $f(z)$ is not conformally invariant due to the correction term $-i \log g'(g^{-1}(z))$ in $f_{\Omega}(z)$. Fig. 4(b) and (c) show examples of the integral curves in Ω .

To study the equilibrium state of the defect motion, we focus on the force acting on two $+1/2$ defects at $z = \pm g(r)$, ($0 < r < 1$). When the defect motion is at equilibrium, the total force applied to each defect should be equal to zero. By calculating the residues of $f'_{\Omega}(z)^2$ and $h'_{\Omega}(z)^2$ around the defect at $z = +g(r)$, the elastic and active forces applied to the defect at $z = +g(r)$ can be calculated from (13) as follows:

$$F_x - iF_y = \frac{\pi K}{g'(r)} \left[\frac{1 - 5r^4 - 2\hat{\alpha}}{4r(1 - r^4)} + \frac{3g''(r)}{4g'(r)} \right], \quad (34)$$

where $\hat{\alpha} \equiv \alpha/K$. By setting the above force (34) equal to zero, we obtain the following equation to satisfy the equilibrium condition:

$$\frac{1 - 5r^4 - 2\hat{\alpha}}{4r(1 - r^4)} + \frac{3g''(r)}{4g'(r)} = 0 \quad (35)$$

Thus, the equilibrium point $z = +g(r)$ is calculated by solving (35) with respect to r and mapping the solution by $g(\zeta)$. The equilibrium point depends on the parameter $\hat{\alpha}$. Conversely, if we obtain the equilibrium point $+g(r)$ from experiments, the parameter $\hat{\alpha}$ can be explicitly estimated from (35) as follows:

$$\hat{\alpha} = \frac{1 - 5r^4}{2} + \frac{3}{2} r(1 - r^4) \frac{g''(r)}{g'(r)} \quad (36)$$

6 Estimation of active stress parameter from cell culture experiments

We demonstrate the validity of the proposed estimation method for the active stress parameter $\hat{\alpha}$ using two existing studies^{16,20} which observed the alignment of mouse myoblast cells (C2C12 cells) in closed domains. In our previous study,²⁰ we considered the domain Ω mapped from the unit disk \mathbb{D} by the function $z = g(\zeta) = \zeta + \beta \zeta^3$ ($0 \leq \beta < 1/3$) as shown in Fig. 5(a). Note that the area of the domain Ω was normalized to that of the unit disk \mathbb{D} , and the length scale in the experiments was normalized by taking 300 μm to be equal to 1, as in the previous study.²⁰

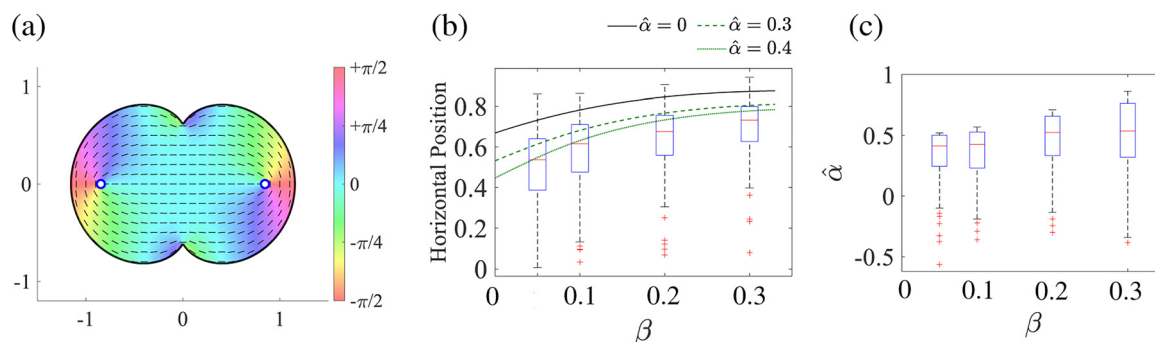


Fig. 5 Estimation of the parameter $\hat{\alpha}$ from the experiments of stable defect positions in mouse myoblast cells.²⁰ (a) Cell alignment in the domain Ω mapped from the unit disk \mathbb{D} by the function $g(\zeta) = \zeta + \beta \zeta^3$. Note that the area of the domain Ω is normalized to that of the unit disk \mathbb{D} . Blue circles represent $+1/2$ defects. (b) Box plots of horizontal defect positions for various geometrical parameters β . (c) Box plots of the predicted parameter $\hat{\alpha}$ from (38). Red cross marks indicate outliers. We used Chebfun⁴⁴ for calculating the inverse map $\zeta = g^{-1}(z)$.



From (35), the equilibrium point $z = +g(r)$ is calculated by solving the following algebraic equation.

$$\frac{1 - 5r^4 - 2\hat{\alpha}}{4r(1 - r^4)} + \frac{18\beta r}{4(1 + 3\beta r^2)} = 0. \quad (37)$$

Fig. 5(b) shows the calculated equilibrium point for $0 \leq \beta < 1/3$ and the experimental results from our previous study, which investigated defect positions in mouse myoblast cells.²⁰ The experimental results are smaller than the theoretically calculated positions without active stress ($\hat{\alpha} = 0$). As the active stress increases ($\hat{\alpha} = 0.3, 0.4$), the theoretical and experimental results become matched. According to (36), the estimation formula for $\hat{\alpha}$ is given as follows:

$$\hat{\alpha} = \frac{1 - 5r^4}{2} + \frac{9\beta r^2(1 - r^4)}{1 + 3\beta r^2}. \quad (38)$$

Fig. 5(c) shows box plots of the estimated parameter $\hat{\alpha}$, whose median is around 0.4 to 0.5. The interquartile range increases as the geometrical parameter β increases, which indicates the uncertainty of the estimation tends to increase as the geometry becomes more asymmetric.

Other work by Ienaga *et al.*¹⁶ considered two overlapping circular boundaries, mathematically modeled as quadrature domains and expressed by the following conformal mapping from the unit disk \mathbb{D} :³⁴

$$z = g(\zeta) = \frac{a^4 - 1}{a^2 - a + 1} \cdot \frac{\zeta}{a^2 - \zeta^2}, \quad (39)$$

where $a > 1$. Fig. 6(a) shows an example of cell alignment in the quadrature domain. According to cell culture experiments,¹⁶ the distance D_{++} between the two $+1/2$ defects was fitted by the distance Δ_q between the centers of the two circles as follows:

$$D_{++} = 2\left(0.58 + \frac{\Delta_q}{2}\right), \quad (40)$$

where the distance Δ_q is expressed as

$$\Delta_q = 2g(1/a) = \frac{2a}{a^2 - a + 1}. \quad (41)$$

On the other hand, the equilibrium point $z = +D_{++}/2 = +g(r)$ is theoretically calculated by solving the following equation:

$$\frac{1 - 5r^4 - 2\hat{\alpha}}{4r(1 - r^4)} + \frac{6r(r^2 + 3a^2)}{4(a^4 - r^4)} = 0. \quad (42)$$

Fig. 6(b) shows the experimental and theoretical distances D_{++} between the two $+1/2$ defects in terms of the distance Δ_q . Similarly to Fig. 5, the experimental values are lower than the theoretical values without active stress ($\hat{\alpha} = 0$). It follows from (42) that the parameter $\hat{\alpha}$ is estimated by the following equation.

$$\hat{\alpha} = \frac{1 - 5r^4}{2} + \frac{3r^2(r^2 + 3a^2)(1 - r^4)}{a^4 - r^4}. \quad (43)$$

The estimated parameter $\hat{\alpha}$ ranged between 0.1 and 0.5 and varied with the distance Δ_q (Fig. 6(c)).

In the above two examples, the parameter $\hat{\alpha}$ is estimated to be positive, which implies that the myoblast cells generate contractile stress. These results are consistent with an existing study on the defect dynamics in free space, which reported that the direction of defect motion in C2C12 cells was opposite to that in neural progenitor cells, which show extensile active behaviors.¹¹ Thus, the proposed estimation method shows promise for quantifying the degree of contractility or extensibility of cell populations using only the equilibrium states of defects. In contrast to an existing study of the quantification of active nematics which considered an integer defect in a small circle,⁴⁵ the proposed method can be applied to arbitrary simply connected domains. This advantage helped reveal the possibility that the active stress parameter $\hat{\alpha}$ depends on the domain geometry (Fig. 5 and 6). However, the uncertainty of the estimated $\hat{\alpha}$ was very large in Fig. 5 and 6. In particular, the estimated $\hat{\alpha}$ changed by a factor of five in Fig. 6, possibly because the experimental results of the distance D_{++} was fitted by a simple line in the study¹⁶ and the error of the fitting is not considered in the estimation of $\hat{\alpha}$. In addition to the explicit formulas for the estimation of $\hat{\alpha}$ (38) and (43), some statistical approaches will also be necessary to capture the distributions of observed defects for a more precise estimation of $\hat{\alpha}$, which will be a focus of our future work. Though further experimental

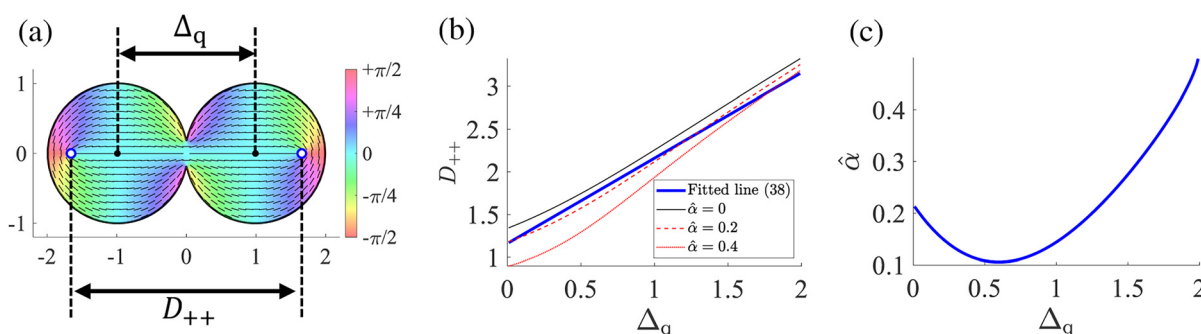


Fig. 6 Estimation of the parameter $\hat{\alpha}$ from the experiments of stable defect positions in mouse myoblast cells in the domain where two disks intersect.¹⁶ (a) Cell alignment in the domain Ω mapped from the unit disk \mathbb{D} by the function (39). Blue circles represent $+1/2$ defects. (b) Distance D_{++} between the two $+1/2$ defects for various geometrical parameters Δ_q . For each Δ_q , the parameter a is obtained by solving (41). (c) Predicted parameter $\hat{\alpha}$ from (43) with a parameter r obtained by solving $D_{++}/2 = g(r)$.



research is needed to validate the estimated parameter $\hat{\alpha}$, our theory revealed that the force acting on a defect can be expressed as residues of complex functions and enabled a detailed analysis of defect dynamics and the estimation of the activeness, which cannot be achieved by numerical simulations. Thus, the proposed theory will open up an analytical approach for investigating the essential dynamics of topological defects in active nematics.

7 Conclusions

This paper proposed a new theoretical framework to mathematically model defect motion by constructing integral curves defined from the director field of a dry active nematic system based on complex analysis. As a result, we revealed that defect motion is characterized by the residues of two holomorphic functions derived from the director field. Moreover, the proposed method reproduced and refined the theory of defect motion for a defect pair and was able to estimate the active stress from the results of cell culture experiments.

In this paper, we modeled the density of active nematic liquid crystals as the densities of integral lines of the holomorphic director field to qualitatively consider the increase and decrease of cell densities around $+1/2$ and $-1/2$ defects, respectively. However, we could not offer an evaluation or comparison of the line densities in the experiments because the size of the nematic liquid crystals is neglected in the proposed theory whereas the size of cells should be considered in actual experiments. An additional limitation is that the spatial variation of the density of the proposed integral lines cannot be controlled and thus the proposed integral lines cannot be precisely fitted to the experimental data because the spatial distributions of the integral lines are determined by the complex function $f(z)$, which is derived from the director field \mathbf{n}_d under the one constant approximation. Thus, further analytic tools are required to bridge the gap between the proposed theoretical model and actual cell experiments to investigate how the density variations affect the defect dynamics.

For the analysis of the defect dynamics, we considered torque-free motion of a defect pair and ignored the direction of the defects in this paper. However, many studies have found that torques around defects play an important role in the complex dynamics of defect motion.^{25,26,28,29,38} Thus, our future work will include an extension of the proposed theory to include the effects of torques around defects. In addition, cell culture experiments are required to verify the theoretical predictions of defect motion and estimated active stress parameter $\hat{\alpha}$.

Author contributions

H. Miyazako: conceptualization, formal analysis, resources, writing original draft; H. Miyoshi: conceptualization, formal analysis, writing original draft; T. N.: conceptualization, supervision, review & editing. All authors gave final approval for

publication and agree to be held accountable for the work performed therein.

Conflicts of interest

There are no conflicts to declare.

Data availability

The program code for this study is available in Zenodo and can be accessed via this link <https://doi.org/10.5281/zenodo.15779307>.

Acknowledgements

The first author was supported in part by the Japan Society for the Promotion of Science KAKENHI (grant numbers JP23H00086 and JP23H04406) and JST, PRESTO Grant Number JPMJPR24KB, Japan. The second author was supported by a Postdoctoral Research Fellowship from the Japan Society for the Promotion of Science (JSPS-24KJ0041).

References

- 1 A. Doostmohammadi, J. Ignés-Mullol, J. M. Yeomans and F. Sagués, *Nat. Commun.*, 2018, **9**, 3246.
- 2 J. Zhao, U. Gulan, T. Horie, N. Ohmura, J. Han, C. Yang, J. Kong, S. Wang and B. B. Xu, *Small*, 2019, **15**, e1900019.
- 3 A. Doostmohammadi and B. Ladoux, *Trends Cell Biol.*, 2022, **32**, 140–150.
- 4 T. Sanchez, D. T. N. Chen, S. J. DeCamp, M. Heymann and Z. Dogic, *Nature*, 2012, **491**, 431–434.
- 5 J. Hardoüin, R. Hughes, A. Doostmohammadi, J. Laurent, T. Lopez-Leon, J. M. Yeomans, J. Ignés-Mullol and F. Sagués, *Commun. Phys.*, 2019, **2**, 121.
- 6 A. J. Tan, E. Roberts, S. A. Smith, U. A. Olvera, J. Arteaga, S. Fortini, K. A. Mitchell and L. S. Hirst, *Nat. Phys.*, 2019, **15**, 1033–1039.
- 7 A. Sciortino, L. J. Neumann, T. Krüger, I. Maryshev, T. F. Teshima, B. Wolfrum, E. Frey and A. R. Bausch, *Nat. Mater.*, 2023, **22**, 260–268.
- 8 I. Vélez-Cerón, P. Guillamat, F. Sagués and J. Ignés-Mullol, *Proc. Natl. Acad. Sci. U. S. A.*, 2024, **121**, e2312494121.
- 9 G. Duclos, C. Erlenkämper, J.-F. Joanny and P. Silberzan, *Nat. Phys.*, 2017, **13**, 58–62.
- 10 T. B. Saw, A. Doostmohammadi, V. Nier, L. Kocgozlu, S. Thampi, Y. Toyama, P. Marcq, C. T. Lim, J. M. Yeomans and B. Ladoux, *Nature*, 2017, **544**, 212–216.
- 11 K. Kawaguchi, R. Kageyama and M. Sano, *Nature*, 2017, **545**, 327–331.
- 12 P. Guillamat, C. Blanch-Mercader, G. Pernollet, K. Kruse and A. Roux, *Nat. Mater.*, 2022, **21**, 588–597.
- 13 V. Yashunsky, D. J. G. Pearce, C. Blanch-Mercader, F. Ascione, P. Silberzan and L. Giomi, *Phys. Rev. X*, 2022, **12**, 041017.
- 14 J.-M. Armengol-Collado, L. N. Carenza, J. Eckert, D. Krommydas and L. Giomi, *Nat. Phys.*, 2023, **19**, 1773–1779.



- 15 K. Kaiyrbekov, K. Endresen, K. Sullivan, Z. Zheng, Y. Chen, F. Serra and B. A. Camley, *Proc. Natl. Acad. Sci. U. S. A.*, 2023, **120**, e2301197120.
- 16 R. Ienaga, K. Beppu and Y. T. Maeda, *Soft Matter*, 2023, **19**, 5016–5028.
- 17 T. Sarkar, V. Yashunsky, L. Brézin, C. Blanch Mercader, T. Aryaksama, M. Lacroix, T. Risler, J.-F. Joanny and P. Silberzan, *PNAS Nexus*, 2023, **2**, gad034.
- 18 M. Riedl, I. Mayer, J. Merrin, M. Sixt and B. Hof, *Nat. Commun.*, 2023, **14**, 5633.
- 19 C.-L. Lv, Z.-Y. Li, S.-D. Wang and B. Li, *Commun. Phys.*, 2024, **7**, 351.
- 20 H. Miyazako, K. Tsuchiyama and T. Nara, *npj Biol. Phys. Mech.*, 2024, **1**, 1.
- 21 Y. Maroudas-Sacks, L. Garion, L. Shani-Zerbib, A. Livshits, E. Braun and K. Keren, *Nat. Phys.*, 2021, **17**, 251–259.
- 22 Z. Wang, M. C. Marchetti and F. Brauns, *Proc. Natl. Acad. Sci. U. S. A.*, 2023, **120**, e2220167120.
- 23 L. Giomi, M. J. Bowick, P. Mishra, R. Sknepnek and M. Cristina Marchetti, *Philos. Trans. R. Soc., A*, 2014, **372**, 20130365.
- 24 A. J. Vromans and L. Giomi, *Soft Matter*, 2016, **12**, 6490–6495.
- 25 X. Tang and J. V. Selinger, *Soft Matter*, 2017, **13**, 5481–5490.
- 26 X. Tang and J. V. Selinger, *Soft Matter*, 2019, **15**, 587–601.
- 27 A. H. Lewis, D. G. A. L. Aarts, P. D. Howell and A. Majumdar, *Stud. Appl. Math.*, 2017, **138**, 438–466.
- 28 F. Vafa, M. J. Bowick, M. C. Marchetti and B. I. Shraiman, arXiv, 2020, preprint, [cond-mat.soft], DOI: [10.48550/arXiv.2007.02947](https://doi.org/10.48550/arXiv.2007.02947).
- 29 F. Vafa, *Soft Matter*, 2022, **18**, 8087–8097.
- 30 O. S. Tarnavskyy, M. F. Ledney and A. I. Lesiuk, *Liq. Cryst.*, 2018, **45**, 641–648.
- 31 O. S. Tarnavskyy and M. F. Ledney, *Liq. Cryst.*, 2023, **50**, 21–35.
- 32 H. Miyazako and T. Nara, *R. Soc. Open Sci.*, 2022, **9**, 211663.
- 33 H. Miyazako and T. Sakajo, *Proc. R. Soc. A*, 2024, **480**, 20230879.
- 34 H. Miyoshi, H. Miyazako and T. Nara, *Proc. R. Soc. A*, 2024, **480**, 20240405.
- 35 T. G. J. Chandler and S. E. Spagnolie, *J. Fluid Mech.*, 2023, **967**, A19.
- 36 T. G. J. Chandler and S. E. Spagnolie, *SIAM J. Appl. Math.*, 2024, **84**, 2476–2501.
- 37 J. Rønning, C. M. Marchetti, M. J. Bowick and L. Angheluta, *Proc. R. Soc. A*, 2022, **478**, 20210879.
- 38 S. Čopar and Ž. Kos, *Soft Matter*, 2024, **20**, 6894–6906.
- 39 P. G. de Gennes and J. Prost, *The physics of liquid crystals*, Clarendon Press, Oxford, England, 2nd edn, 1995.
- 40 V. Vitelli and D. R. Nelson, *Phys. Rev. E: Stat., Nonlinear, Soft Matter Phys.*, 2006, **74**, 021711.
- 41 C. Denniston, *Phys. Rev. B: Condens. Matter Mater. Phys.*, 1996, **54**, 6272–6275.
- 42 H. Miyoshi, D. G. Crowdy, H. Miyazako and T. Nara, *Proc. R. Soc. A*, 2025, **481**, 20240569.
- 43 R. Aditi Simha and S. Ramaswamy, *Phys. Rev. Lett.*, 2002, **89**, 058101.
- 44 T. A. Driscoll, N. Hale and L. N. Trefethen, *Chebfun Guide*, Pafnuty Publications, 2014.
- 45 C. Blanch-Mercader, P. Guillamat, A. Roux and K. Kruse, *Phys. Rev. Lett.*, 2021, **126**, 028101.

